International Journal of Modelling and Simulation

ISSN: 0228-6203 (Print) 1925-7082 (Online) Journal homepage: www.tandfonline.com/journals/tjms20

Analysis, design and implementation of direct torque controlled induction motor drive based on slip angle

K. V. Praveen Kumar, T. Vinay Kumar & S. Srinivasa Rao

To cite this article: K. V. Praveen Kumar, T. Vinay Kumar & S. Srinivasa Rao (2017) Analysis, design and implementation of direct torque controlled induction motor drive based on slip angle, International Journal of Modelling and Simulation, 37:4, 208-219, DOI: 10.1080/02286203.2017.1327295

To link to this article: https://doi.org/10.1080/02286203.2017.1327295

INTERNATIONAL JOURNAL OF MODELLING AND SIMULATION, 2017
VOL. 37, NO. 4, 208–219
https://doi.org/10.1080/02286203.2017.1327295

Taylor & Francis
Taylor & Francis Group

Analysis, design and implementation of direct torque controlled induction motor drive based on slip angle

K. V. Praveen Kumar, T. Vinay Kumar and S. Srinivasa Rao

Electrical Engineering Department, National Institute of Technology, Warangal, India

ABSTRACT

The conventional direct torque control (DTC) of induction motor drive has two main problems such as higher ripple in torque, flux and variable switching frequency. These problems are mainly due to the hysteresis controllers. Appreciable reduction of torque and flux ripple can be achieved by increasing the inverter switching frequency. Most of the torque ripples reduction methods in literature are centered on this concept. The hysteresis based approach also results in variable switching frequency that depends on operating conditions at particular speed. Hence a method for increasing the switching frequency and at the same time maintaining constant switching frequency is needed. Most researches have chosen the space vector pulse width modulation based DTC (SVM-DTC) scheme. In this paper, first the torque and flux ripple in the conventional DTC method are shown and the improvement achieved by using proposed DTC method based on slip angle is presented. A new method such as slip angle control of induction motor drive based on DTC are proposed, analyzed, simulated, and tested. It is shown that this method progressively reduces torque and flux ripple.

ARTICLE HISTORY
Received 14 April 2016
Accepted 3 May 2017

KEYWORDS
Control of electrical drive; direct torque control; direct flux control; induction motor drive; speed PI controller design; torque PI controller design; two-level voltage source inverter

1. Introduction

Induction motor speed control methods can be classified into scalar control and vector control methods. In scalar control, only magnitude and frequency of voltage, flux and current space vectors are controlled. Scalar control does not act on space vectors during transients. Contrarily, in vector control not only magnitude and frequency but also instantaneous positions of voltage, flux and current space vectors are controlled. Thus, vector control acts on the position of space vectors and provides their correct orientation both at steady state and also during transients. The invention of vector control in the beginning of 1970s brought a revival in the performance and control of induction motor drives. Vector control is also known as field oriented control (FOC) [1], it has several limitations: torque control is indirect, current regulators are required, coordinate transformation is required and the PWM modulator, which processes the voltage and frequency reference outputs of the vector control stage, creates a delay between the input references and the resulting stator voltage vector produced. These factors limit the ability of FOC to achieve rapid flux and torque control. To eliminate these limitations, in 1986 Takahashi and Noguchi proposed a technique called direct torque control (DTC) [2]. However, the conventional DTC method has limitations. Large torque and flux ripples are generated particularly at low speeds [3–6]. To address these problems, switching frequency of the inverter has to be kept constant for improving steady state torque and flux response of induction motor drive by using Space Vector Modulation (SVM) DTC technique [7]. SVM-DTC preserves conventional DTC transient virtues furthermore it produces better quality in steady-state flux and torque response over a wide speed range. At each control cycle, SVM technique uses the reference voltage space vectors to compensate the stator flux and torque errors [8,9]. In [10], proposed a technique to increase the performance of DTC at low speed operation by modified inverter switching table of conventional DTC, but switching frequency is uncontrolled. In [11–13] new techniques called dithering was implemented, which increases the switching frequency of inverter. These techniques, allow lifting the inverter switching frequency to get silent motor operation, but it requires high sampling frequency than SVM-DTC and the variable switching frequency problem remains unsolved. A modified DTC technique was proposed [14] to maintain constant switching frequency. But it is difficult to implement in digital control. Based on current ripple principle in [15] a new DTC technique was proposed for three-level inverter to reduce the torque ripple and flux ripple, but switching frequency is still function of induction motor speed. In [16], DTC technique was implemented with five-level output voltage from the inverter to improve the low speed performance and also reduces the torque and flux ripple. But it needs the stator flux angle position and trigonometric function calculations in modulation unit. Multilevel voltage source inverters increase the cost and control complexity [17,18]. In order to reduce the computational complexity and parameter sensitivity with low flux and torque ripple, a prediction DTC

CONTACT T. Vinay Kumar vinaykumar@nitw.ac.in

scheme was proposed in [19]. For digital implementation it also requires high sampling frequency when compared to conventional DTC. In [20], a new DTC technique was proposed to improve the steady state response of flux and torque. But it requires several complicated calculations and inverter switching problem is unsolved. In [21], an accurate estimation method to overcome the limitations of the existing speed and flux estimation methods is proposed. It has been concluded by sensitivity analysis. In [22], an estimation technique for motor parameters like stator resistance and rotor resistance by using fuzzy logic control was developed. But speed control technique has not been considered in this method. In order to reduce the energy losses in induction motor drive in [23] authors proposed a new soft starting technique by using neuro-fuzzy method. But, as paper is confined to starting transients, the performance analysis in steady state has not been addressed. In [24], the sensor-less DTC based induction motor drive is discussed in detail, but it requires complex calculations to estimate controller parameters, co-ordinate transformation and sector identification. From the literature survey it is observed that available control schemes have various advantages and drawbacks. However, most of the existing control techniques are concentrated to operate the inverter with constant switching frequency. The detailed torque and flux control law is not properly presented and also the mathematical equations which are required to determine the inverter switching sequence are not clearly described. Consequently, the undesired torque and flux ripple in DTC based induction motor drives may lead to speed oscillations, resonances in mechanical portions of the drive causing noise and vibration. Hence torque and flux ripple should be reduced.

The objectives of this research paper are to: Propose better scheme for DTC induction motor drive to reduce torque ripple and flux ripple, develop mathematical models for the proposed scheme, design and develop torque and flux PI controllers for the proposed scheme, carry out simulation studies on the proposed scheme, compare the simulation results of proposed schemes with existing schemes and validate the proposed schemes by conducting experiments. In proposed DTC slip angle control technique, the required reference stator flux space vector is generated from the controlled stator flux slip angle and measured rotor angle of the induction motor drive. In this scheme, torque equation is derived in terms of stator flux angle. In proposed DTC scheme, coordinate transformation is not required; all mathematical calculations are done in the stator reference frame. This proposed method is extension of the author previous work [27]. For the proposed DTC scheme detailed simulation and experimental results are presented and significances are highlighted. The steady state and transient behavior of the proposed DTC scheme based on slip angle control is compared with conventional DTC for analyzing the response of torque and flux.

2. Control strategy

The detailed block diagram of proposed DTC scheme based on slip angle control is shown in Figure 1. In Figure 1, the speed reference is compared with the measured speed, speed error is given to PI controller and it generates reference torque. The reference stator flux is obtained from the speed reference. The reference torque is compared with estimated torque and the error is the input to torque PI controller, it generates reference slip angle in this proposed DTC scheme. The reference stator flux angle is calculated from the reference slip angle with the help of reference stator flux angle; the required reference stator flux is calculated and compared with the estimated stator flux. Based on the error, the reference voltage is calculated. Finally, the reference voltage space vector is realized by using Kim-Sul SVM [25].

From [26], the modified instantaneous electromagnetic torque T_e is given by:

$$T_e(t) = \left[\frac{3}{2}p\frac{L_m^2}{R_r L_s^2}\left|\psi_s^2\right|\right]\left[1 - e^{-t/\tau}\right]\left(\frac{\mathrm{d}\theta_{slip}}{\mathrm{d}t}\right) \tag{1}$$

If stator flux module $|\psi_s|$ is maintained constant, then Equation (1) can be written in Laplace transformation as

$$T_e(s) = \frac{sk_s}{1 + s\tau_s}.\theta_{slip}(s) \tag{2}$$

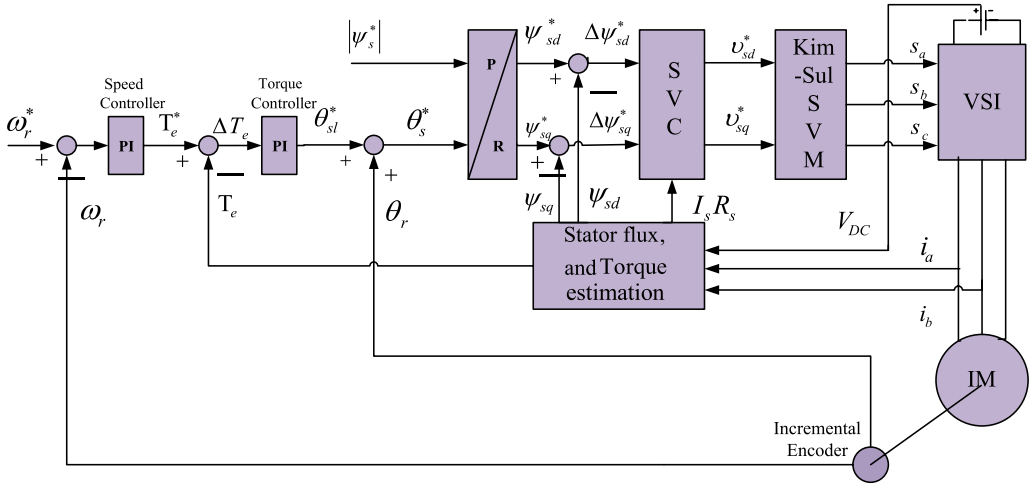

Figure 1. Proposed DTC scheme based on slip angle control.

where k_s is the torque proportionality constant.

Equation (2) shows that the linear relationship between torque and slip angle. Hence the electromagnetic torque T_e is directly controlled by using slip angle for a given sample time Δt.

From [12], stator voltage

$$d\psi_s/dt = V_s - i_s R_s \tag{3}$$

where ψ_s is the stator flux, V_s is the voltage space vector, $i_s R_s$ is the stator winding resistive voltage drop and Δt is the sample time. By neglecting stator winding resistive voltage drop, Equation (3) becomes

$$\Delta\psi_s = V_s \Delta t \tag{4}$$

The torque error ΔT_e can be controlled by slip angle θ_{slip} using Equation (2) and the stator flux error $\Delta\psi_s$ can be controlled by suitable voltage vector V_s for particular sample time Δt using Equation (4). The author's previous [27] work shows how stator flux and torque error are compensated by voltage space vector V_s in a given sample time Δt based on proposed scheme.

If the voltage space vector is in sector-1 as shown in Figure 2 which is at an angle of 'α' with reference to A-phase axis also called as α-axis, the reference vector V_s^* will be realized in the average sense by switching amongst the three nearest vertices of the sector in which the tip of this reference vector lies.

For instance, the switching combinations would be chosen are (8-1-2-7), respectively, switched for the time intervals of $(T_0/2 - T_1 - T_2 - T_0/2)$. As per the conventional SVM, the switching times are given by Equation (5) and its derivation is explained with the help of Equations (6) and (7):

$$T_1 = \frac{m_i T_s \sin(60^\circ - \alpha)}{\sin 60^\circ} \tag{5a}$$

$$T_2 = \frac{m_i T_s \sin\alpha}{\sin 60^\circ} \tag{5b}$$

$$\therefore T_1 = T_s\left[\frac{|V_{sr}| \times \cos\alpha \times \sin 60^\circ) - |V_{sr}| \times \sin\alpha \times \cos 60^\circ)}{V_{dc} \sin 60^\circ}\right] \tag{5c}$$

$$\therefore T_1 = \frac{T_s}{V_{dc}}\left[v_\alpha^* - \frac{v_\beta^*}{\sqrt{3}}\right] \tag{5d}$$

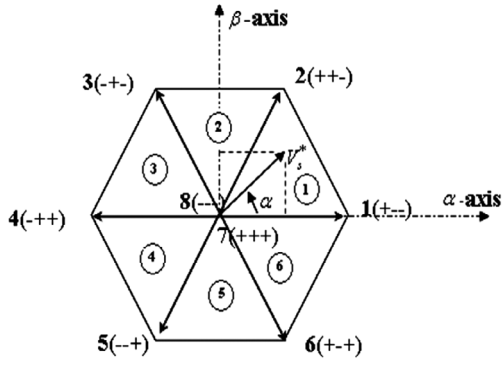

Figure 2. Space phasors corresponding to each switching state.

Since

$$\begin{bmatrix} v_\alpha^* \\ v_\beta^* \end{bmatrix} = \begin{bmatrix} 3/2 & 0 & 0 \\ 0 & \sqrt{3}/2 & -\sqrt{3}/2 \end{bmatrix}\begin{bmatrix} v_a^* \\ v_b^* \\ v_c^* \end{bmatrix} \tag{6a}$$

$$\begin{bmatrix} v_a^* \\ v_b^* \\ v_c^* \end{bmatrix} = \frac{2}{3}\begin{bmatrix} 1 & 0 \\ -1/2 & \sqrt{3}/2 \\ -1/2 & -\sqrt{3}/2 \end{bmatrix}\begin{bmatrix} v_\alpha^* \\ v_\beta^* \end{bmatrix} \tag{6b}$$

$$T_1 = \frac{T_s}{V_{dc}}\left[\frac{3}{2}v_a^* - \frac{1}{\sqrt{3}} \times \frac{\sqrt{3}}{2}(v_b^* - v_c^*)\right] \tag{6c}$$

$$\therefore T_1 = \frac{T_s}{V_{dc}}\left[v_a^* - v_b^*\right] \Rightarrow T_1 = T_{as} - T_{bs} \tag{6d}$$

where $T_{as} = \frac{T_s \times v_a^*}{V_{dc}}$, $T_{bs} = \frac{T_s \times v_b^*}{V_{dc}}$ and $T_{cs} = \frac{T_s \times v_c^*}{V_{dc}}$.

$$T_2 = \frac{m_a T_s \sin\alpha}{\sin 60^\circ} \tag{7a}$$

$$T_2 = \frac{T_s}{V_{dc}} \times \frac{2}{\sqrt{3}}\left[\left(\frac{\sqrt{3}}{2}v_b^* - \frac{\sqrt{3}}{2}v_c^*\right)\right] \tag{7b}$$

$$\therefore T_2 = \frac{T_s}{V_{dc}}\left[v_b^* - v_c^*\right] \Rightarrow T_2 = T_{bs} - T_{cs} \tag{7c}$$

In Equations (6) and (7) T_{as}, T_{bs} and T_{cs} are the switching times, which are proportional to the instantaneous three phase reference voltages and these are termed as the imaginary switching times (8).

$$v_a^* + v_b^* + v_c^* = 0 \Rightarrow T_{as} + T_{bs} + T_{cs} = 0 \tag{8}$$

In sector-1, actual gating times can be calculated as follows and these are given by Equation (9)

$$\text{Max}(T_{as}, T_{bs}, T_{cs}) = T_{as}\ \text{Min}(T_{as}, T_{bs}, T_{cs}) = T_{cs} \tag{9a}$$

$$\Rightarrow T_1 + T_2 = T_{eff} = T_{bs} - T_{cs} \tag{9b}$$

In other words

$$T_{eff} = T_{max} - T_{min} \text{ or } T_0 = T_s - T_{eff} \tag{9c}$$

The actual gate timings are now obtained by simply giving a time shift that would place the effective time exactly at the center of the sampling time interval. This time shift is given [26] as:

$$T_{offset} = \frac{T_0}{2} - T_{min} \tag{9d}$$

Therefore, the actual gate switching timings for the top switching devices of the three-phase inverter are given as Equation (10):

$$\begin{bmatrix} T_{ga} \\ T_{gb} \\ T_{gc} \end{bmatrix} = \begin{bmatrix} 1 & 0 & 0 \\ 0 & 1 & 0 \\ 0 & 0 & 1 \end{bmatrix} \begin{bmatrix} T_{as} \\ T_{bs} \\ T_{cs} \end{bmatrix} + T_{offset} \begin{bmatrix} 1 \\ 1 \\ 1 \end{bmatrix} \quad (10)$$

It is proved that the implementation of the space vector PWM is based on the three instantaneous phase reference voltages (8). Figure 3 shows the pictorial representation of the generation of the switching times from the instantaneous three phase reference voltages. Thus, it is evident that the implementation of this PWM scheme does not require any sector identification, look-up tables etc. The switching sequences are automatically generated which depend on the three phase reference voltages.

The merits of this proposed DTC is

- The required reference voltage vector is calculated from the controlled reference stator flux space vector, which is generated from the proposed torque controller. In this scheme, coordinate transformation is not needed since all mathematical calculations are done in the stator reference frame. The torque is directly controlled by slip angle, which is generated from the proposed torque controller. In this scheme one PI controller is required to control the flux and torque. All reference voltage vectors are calculated in stator reference frame. Hence, coordinate transformation is not required to generate the reference voltage vector and also the required inverter switching states in any sector can be generated by using minimum and maximum values of control time signals, this process does not require information of the reference voltage sector number and trigonometric functions unlike SVM-DTC scheme. Hence, it reduces the computation burden on the processor and improves the performance of the proposed DTC scheme because of digital control process, the performance of the drive not only depends on control scheme but also on computational time.
- The implementation of the scheme is shown to be simple, as it involves only maximum and minimum values of reference voltage vector. Simulation and experimental results will show the merit of the proposed DTC scheme based on slip angle control, i.e. the torque and stator flux ripples are reduced when compared with conventional DTC.

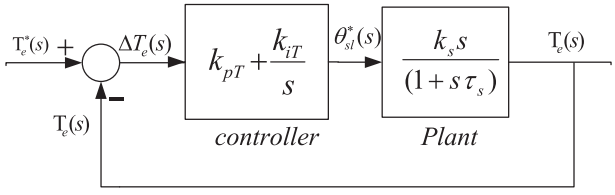

Figure 3a. Block diagram of the torque control loop.

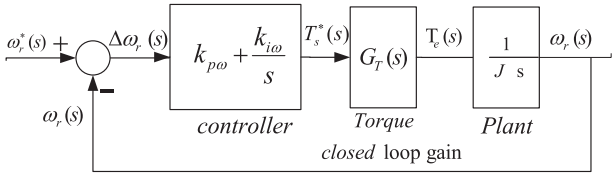

Figure 3b. Block diagram of the speed control loop.

3. Design of PI controllers

The design of parameters required for PI controllers to implement the slip angle control is explained below and parameters of motor drive are described in appendix 1. This proposed scheme is capable of controlling the torque by using slip angle and it also maintains constant stator flux amplitude.

3.1. Torque PI controller

As shown in Figure 1, the reference electromagnetic torque T_e^* is obtained from the speed PI controller output. The reference electromagnetic torque T_e^* is compared with the actual electromagnetic torque T_e to generate a torque error signal. This torque error is the input signal to the torque PI controller. The objective of the torque PI controller is to generate the required slip angle for adjusting the stator flux angle. The relationship between torque and slip angle is expressed in Equation (2). From Equation (2), it is clear that torque response depends on slip angle while keeping stator flux amplitude constant at rated value. The torque control loop block diagram is shown in Figure 3a.

Where $k_s = \frac{3}{2}P(L_m^2/R_rL_s)|\psi_s|^2$, is system gain constant, $\tau_s = \sigma L_r/R_r$ is the system time constant.

The system gain and time constants are given in Equation (11)

$$k_s = \frac{3}{2} \times 2(0.198^2/(1.17 \times 0.23)) = 0.437 \quad (11a)$$

$$\tau_s = \sigma L_r/R_r \quad (11b)$$

In Equation (9) $(\sigma = 1 - L_m^2/L_sL_r = 1 - 0.198^2/(0.23 \times 0.23)) = 0.259)$ and $\tau_s = 0.259 \times (0.23/1.17) = 0.051$.

k_{pT} is the torque controller proportional gain and k_{iT} is the controller integrator constant.

From Figure 3a, the plant output torque can be expressed as Equation (12).

$$T_e(s) = \frac{(k_{pT}s + k_{iT})k_s}{(\tau_s + k_{pT}k_s)s + (1 + k_{iT}k_s)} T_e^* \quad (12)$$

From Equation (12), the characteristic equation can be written as

$$(\tau_s + k_{pT}k_s)s + (1 + k_{iT}k_s) = 0 \quad (13)$$

From Equation (13), the controller gains can be calculated and the gains are given by Equation (14)

$$t_c = (\tau_s + k_{pT}k_s)/(1 + k_{iT}k_s) \quad (14)$$

For first-order systems the settling time $t_s = 5 \cdot t_c$.

Consider settling time $t_s = 0.05$ than time constant $t_c = 0.01$.

Initially choose $k_{pt} = 0.5$ and substitute it in Equation (14), then controller integration constant k_{iT} can be calculated as $0.01 = (0.051 + 0.5 \times 0.437)/(1 + k_{iT} \times 0.437) \Rightarrow k_{iT} = 59$.

Based on these torque control parameters, the speed PI controller parameters design is presented in the next section.

3.2. Speed PI controller

As shown in Figure 1, the reference electromagnetic torque T_e^* is obtained from the speed PI controller output. The reference speed ω_r^* is compared with the measured speed ω_r to generate a speed error signal. This speed error signal is the input to the speed PI controller. The objective of the speed PI controller is to generate the required torque for adjusting the stator flux angle. The relationship between speed and torque is expressed in Equation (15). The speed control loop block diagram is shown in Figure 6.

$$T_e(t) = J\frac{\mathrm{d}\omega_r}{\mathrm{d}t} + B\omega_r + T_l \tag{15}$$

where J is the inertia, B is the friction coefficient and T_l is the load torque.

Assume $T_l = 0$ and B is very low, then Equation (15) becomes as

$$T_e(t) = J\frac{\mathrm{d}\omega_r}{\mathrm{d}t} \tag{16}$$

On applying Laplace transformation to Equation (16), Equation (17) was obtained.

$$\omega_r(s) = \frac{1}{Js}T_e(s) \tag{17}$$

where $G_T(s)$ is the torque closed loop gain, $k_{p\omega}$ is the speed controller proportional gain and $k_{i\omega}$ is the speed controller integration constant and J (0.051 kg m^2) is the inertia of the motor.

The torque closed loop gain can be written as Equation (18)

$$G_T(s) = \frac{T_e(s)}{T_e^*} = \frac{(k_{pT}s + k_{iT})k_s}{(\tau_s + k_{pT}k_s)s + (1 + k_{iT}k_s)} \tag{18}$$

Forward gain of the speed loop is given in Equation (19)

$$G_\omega(s) = \frac{k_{p\omega}(1 + sT_{i\omega})}{sT_{i\omega}} \frac{(k_{pT}s + k_{iT})k_s}{(\tau_s + k_{pT}k_s)s + (1 + k_{iT}k_s)} \cdot \frac{1}{Js} \tag{19}$$

where $T_{i\omega}$ is the speed integral controller time constant.

From Equation (19),

$$G_\omega(s) = \frac{k_{p\omega}(1 + sT_{i\omega})}{sT_{i\omega}} \frac{k_{pT}k_s s + k_{iT}k_s}{(1 + k_{iT}k_s)\left[1 + \frac{(\tau_s + k_{pT}k_s)}{(1 + k_{iT}k_s)}s\right]} \cdot \frac{1}{Js} \tag{20}$$

Substitute $T_{i\omega} = \frac{(\tau_s + k_{pT}k_s)}{(1 + k_{iT}k_s)}$ in the above equation, then forward gain will be given as Equation (21)

$$G_\omega(s) = \frac{k_{p\omega}(k_{pT}k_s s + k_{iT}k_s)}{s(\tau_s + k_{pT}k_s)} \cdot \frac{1}{Js} \tag{21}$$

Overall speed transfer function can be represented by Equation (22)

$$\frac{\omega_r(s)}{\omega_r^*(s)} = \frac{\frac{k_{p\omega}(k_{pT}k_s s + k_{iT}k_s)}{s(\tau_s + k_{pT}k_s)} \cdot \frac{1}{Js}}{1 + \frac{k_{p\omega}(k_{pT}k_s s + k_{iT}k_s)}{s(\tau_s + k_{pT}k_s)} \cdot \frac{1}{Js}} \tag{22}$$

From Equation (22), the characteristic equation can be written as

$$s^2 + \frac{k_{p\omega}k_s k_{pT}}{(\tau_s + k_s k_{pT})J}s + \frac{k_{iT}k_{p\omega}k_s}{(\tau_s + k_s k_{pT})J} = 0 \tag{23}$$

Compare Equation (23) with standard second order characteristic equation; therefore it gives (24)

$$2\zeta\omega_n = \frac{k_{p\omega}k_s k_{pT}}{(\tau_s + k_s k_{pT})J} \text{ and } \omega_n^2 = \frac{k_{iT}k_{p\omega}k_s}{(\tau_s + k_s k_{pT})J} \tag{24}$$

Using Equation (24), the speed $k_{p\omega}$ and $k_{i\omega}$ can be calculated and these are given by Equation (25).

$$2\zeta\omega_n = \frac{k_{p\omega}k_s k_{pT}}{(\tau_s + k_s k_{pT})J} \tag{25a}$$

$$2 * \times 0.707 \times \omega_n = \frac{k_{p\omega} \times 0.437 \times 0.5}{(0.051 + 0.437 \times 0.5) \times 0.05} \Rightarrow k_{p\omega} = 0.087 \times \omega_n \tag{25b}$$

$$\omega_n^2 = \frac{k_{iT}k_{p\omega}k_s}{(\tau_s + k_s k_{pT})J} \tag{25c}$$

$$\omega_n^2 = \frac{59 \times k_{p\omega} \times 0.437}{(0.051 + 0.437 \times 0.5) \times 0.05} \Rightarrow k_{p\omega} = \omega_n^2/1913 \Rightarrow \omega_n = 166.43 \tag{25d}$$

The speed controller gains can be calculated by using Equation (26).

$$k_{p\omega} = 0.078 \times 166.43 \Rightarrow k_{p\omega} = 14.48 \tag{26}$$

and the speed integral controller gain can be calculated as shown in Equation (27)

$$k_{i\omega} = k_{p\omega}/T_{i\omega} \Rightarrow k_{i\omega} = k_{p\omega}/\frac{(\tau_s + k_{pT}k_s)}{(1 + k_{iT}k_s)} \tag{27a}$$

$$k_{i\omega} = 14.48/\frac{(0.051 + 0.5 \times 0.437)}{(1 + 52.31 \times 0.437)} \Rightarrow k_{i\omega} = 1448 \tag{27b}$$

The speed controller gains are given by $k_{p\omega} = 14.48$ and $k_{i\omega} = 1448$.

The presently tested control system response is shown in Figure 4a.

Table 1. Attributes of the step responses of the torque PI controller.

K_{pt}	K_{it}	t_s (s)	% overshoot
0.001	10.8	0.016	25
0.005	11.2	0.013	12.5
0.08	18.7	0.012	6.725
0.06	16.7	0.015	5.625
0.05	15.7	0.0155	5.25
0.03	13.7	0.016	6.625
0.01	11.7	0.0165	10.625

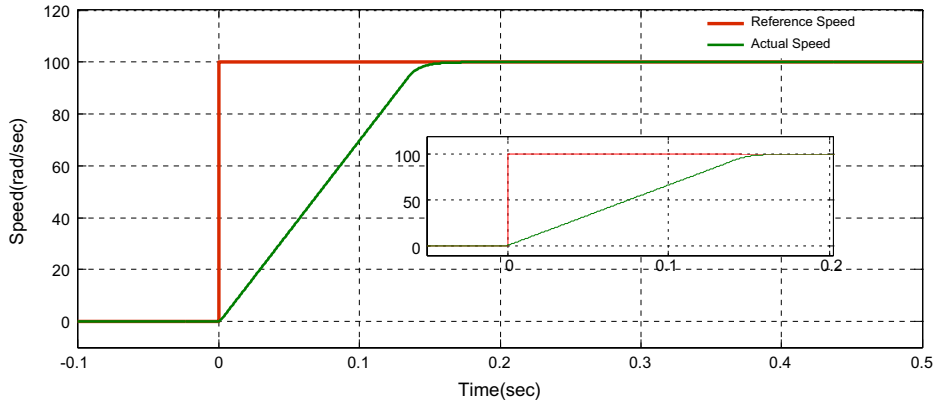

Figure 4a. Step response of the closed loop speed control system for 40% of load torque.

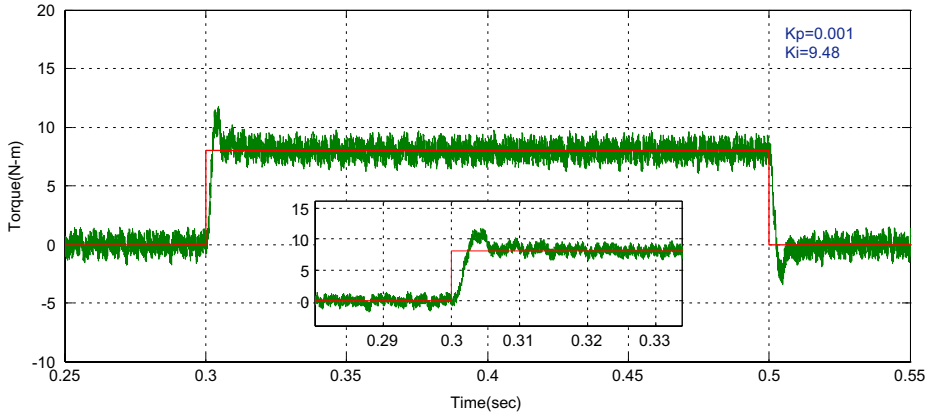

Figure 4b. Step load response of torque loop with $K_p = 0.001$ and $K_i = 10.8$.

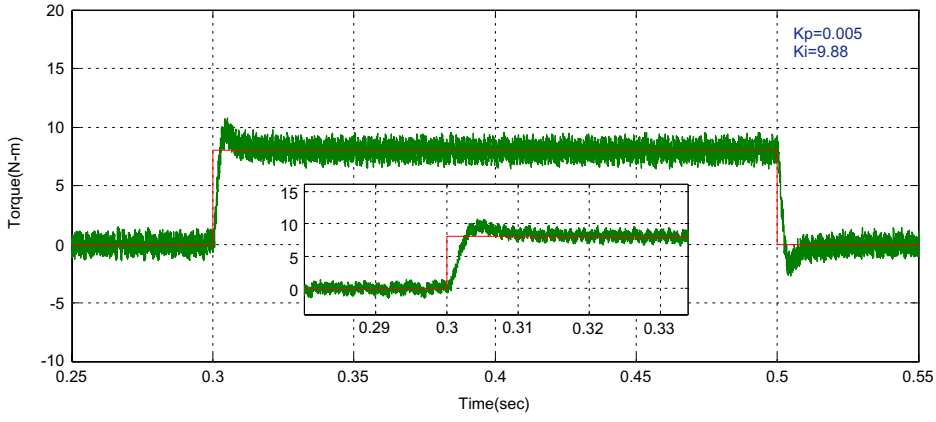

Figure 4c. Step load response of torque loop with $K_p = 0.005$ and $K_i = 11.2$.

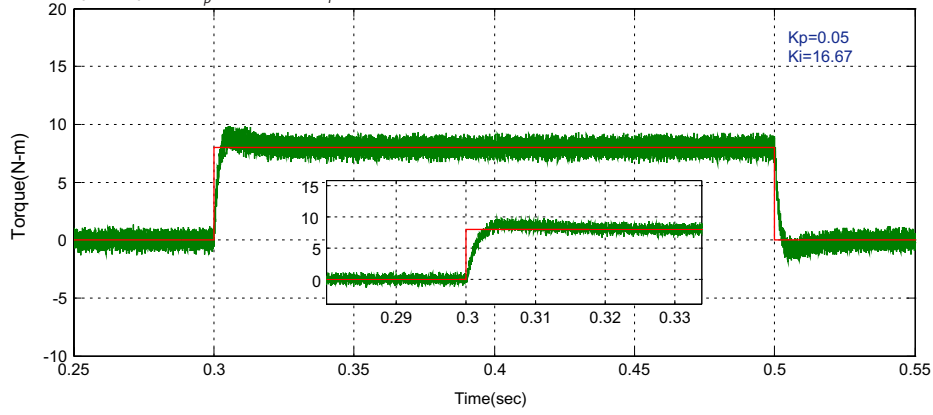

Figure 4d. Step load response of torque loop with $K_p = 0.05$ and $K_i = 15.7$.

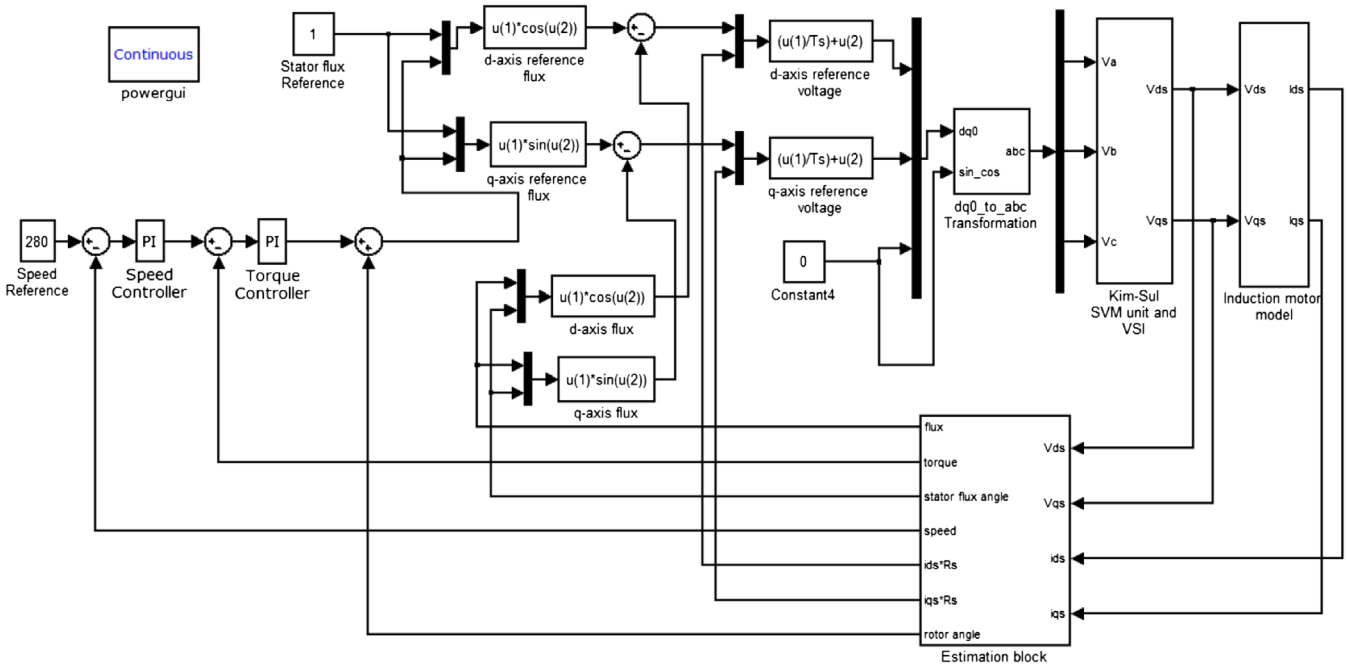

Figure 5. Simulation diagram for proposed DTC scheme based on slip angle control.

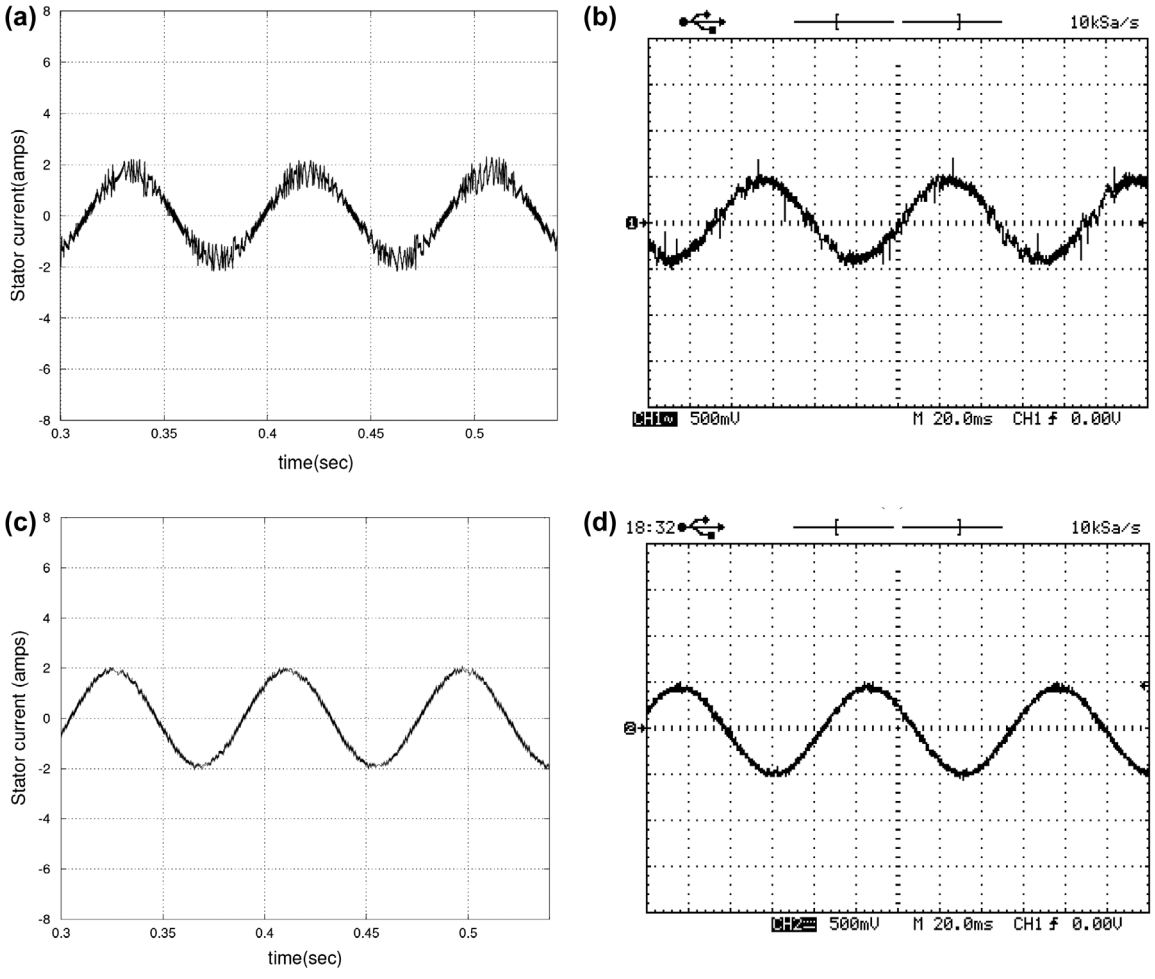

Figure 6. Stator current Ia (2 amps/div): (a) simulation result of conventional DTC, (b) experimental results of conventional DTC, (c) simulation result of proposed DTC and (d) experimental result of proposed DTC.

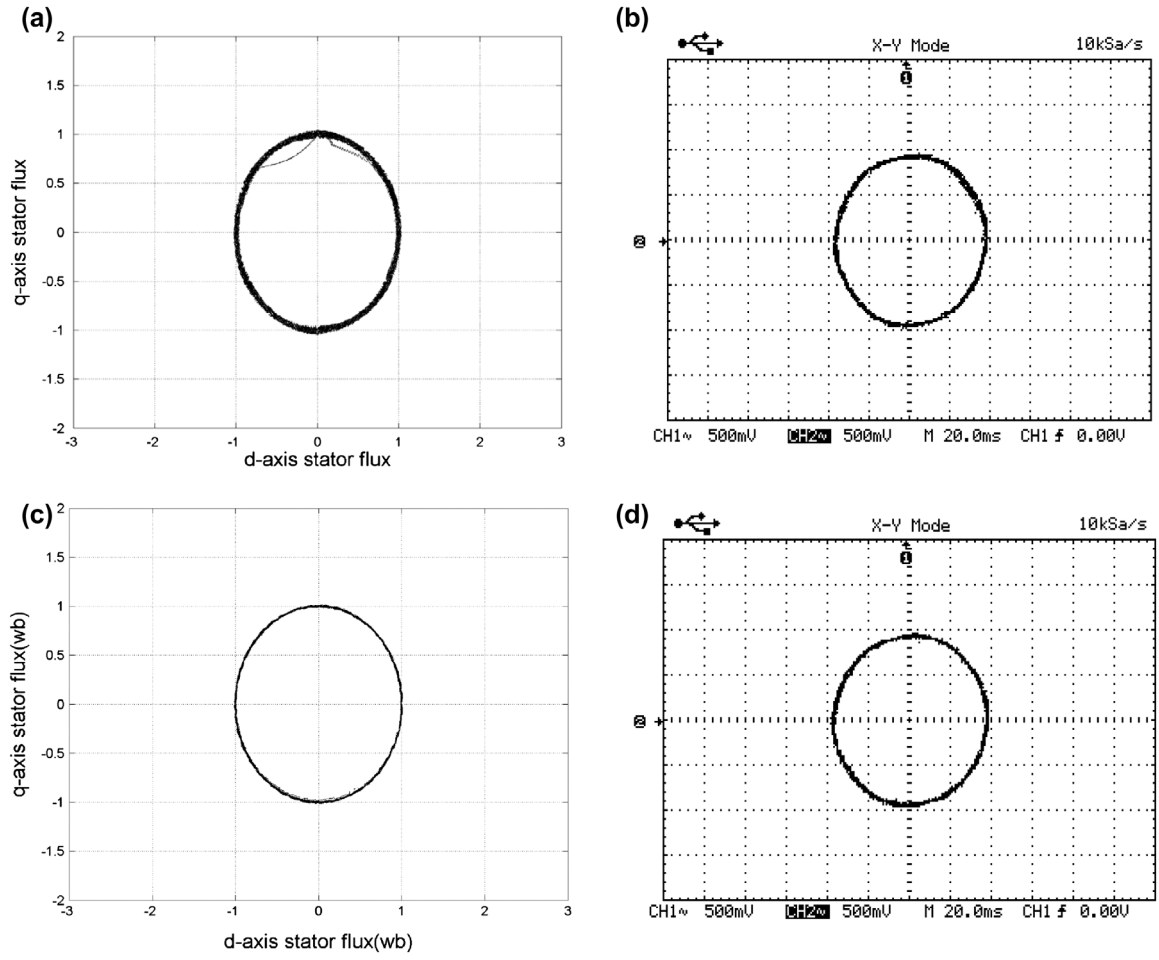

Figure 7. Stator flux locus (0.5 wb/div): (a) simulated response of conventional DTC, (b) experimental reponse of conventional DTC, (c) simulated response of proposed DTC and (d) experimental response of proposed DTC scheme based on slip angle control.

As analyzed in last section, speed controller parameters are adequate for speed control. But in torque PI controller design method assumptions are considered while designing the parameters, which may not give exact adequate PI controller parameters. Therefore, torque PI controller has to be adopted and it parameters are adjusted to k_{pT} = 0.05 and k_{iT} = 16.67. These torque PI controller values gives minimum settling time and low percentage overshoots. As a sample of reference, three different torque PI controller combinations are presented here.

Figure 4 represents effect of K_{pt} and K_{it} on performance of induction machine and the effect of various values of K_{pt} and K_{it} on settling time and percentage overshoot was summarized in Table 1. From Table 1, K_{pt} = 0.05 and K_{it} = 15.67 give minimum settling time and low % overshoot.

4. Modeling

The developed mathematical models and proposed algorithms are simulated using MATLAB/SIMULINK. The simulation diagram of the proposed DTC is shown in Figure 5. The speed controller proportional gain $k_{p\omega}$ is 14.48 and integral gain $k_{i\omega}$ is 1448 and torque controller proportional gain k_{pt} is 0.05 and integral gain k_{it} is 15.7. It is found that these values result in minimum steady-state error; hence all simulation and experimental tests are performed from the obtained values of PI controllers.

5. Simulation and experimental results of slip angle control scheme

The operation of the induction motor drive system is observed at steady state and during transient by sudden application of load. To validate simulation results experiments are conducted for same loaded conditions as applied during simulation process. In order to implement the proposed control schemes for DTC of induction motor drive in real-time a dSpace DS1104 R & D control board is used as an interface between MATLAB/SIMULINK/RTI model and induction motor drive. Simulink models for proposed control scheme are developed. To connect Simulink model to the induction motor drive, it is necessary to introduce I/O interfaces into the model using dSPACE RTI blocks. This will allow the simulation to interface with connected hardware components. A model was created with Simulink and RTI blocks using the Simulink® CoderTM (formerly Real-Time Workshop®). This generates C code. The RTI build process compiles the generated C code and links the object files and libraries into an executable application and loads the application to the

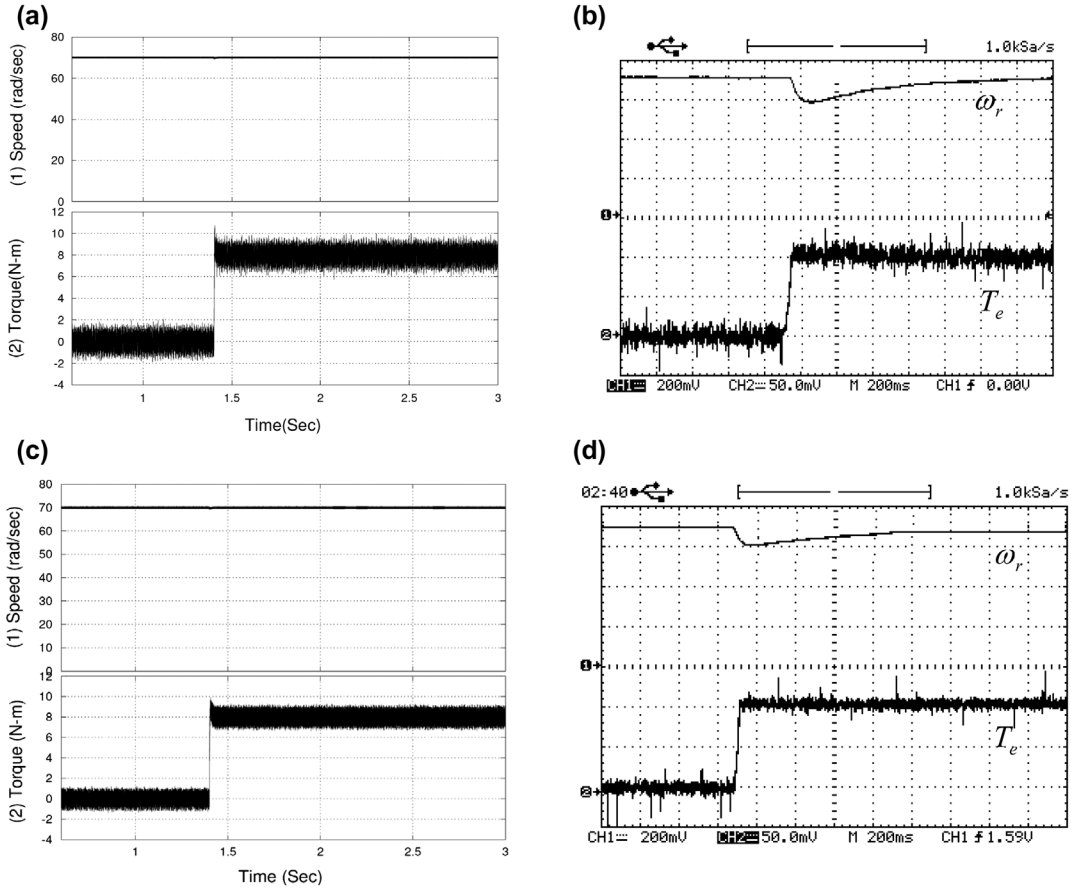

Figure 8. Rotor speed ω_r (20 rad/s/div) and torque T_e (4 N m/div) of induction motor drive: (a) simulated response of conventional DTC, (b) experimental response of conventional DTC, (c) simulated response of proposed DTC and (d) experimental response of proposed DTC scheme based on slip angle control.

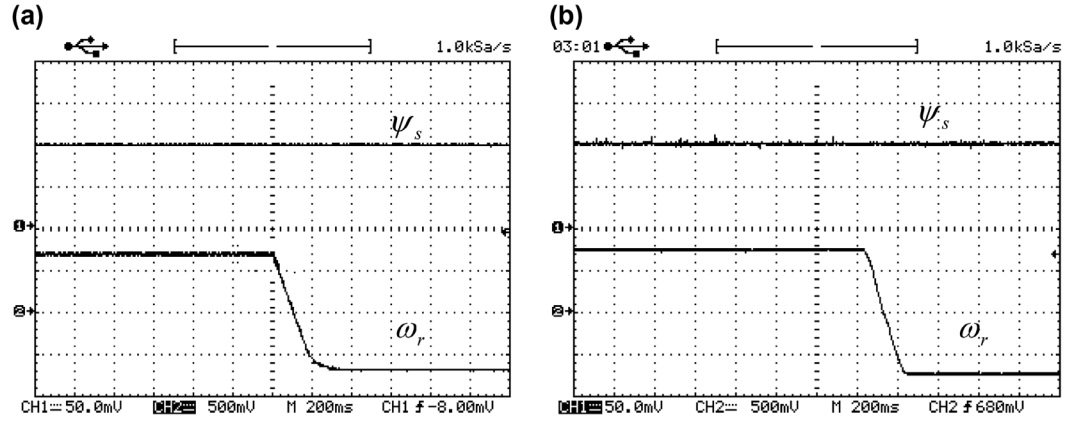

Figure 9. Stator flux ψ_s (0.5 wb/div) and rotor speed ω_r (50 rad/s/div) of Induction motor drive: (a) experimental results of conventional DTC, (b) experimental results of proposed DTC scheme based on slip angle control.

real-time hardware directly after the compilation (build). The build status is displayed in the MATLAB Command Window and generates the four files namely PPC: The real-time application to be downloaded to a PowerPC board, MAP: Map file with address information of variables, TRC: Variable description files to be used by Control Desk, SDF: System description files with references to the PPC, MAP, and TRC file. Using the information from the SDF file the Control Desk can read and write the variables in real-time.

Control Desk provides numerous instruments with their control knobs to measure the variables, to control the variables, to view the output and to change the scale of the output parameter displayed. The values of various parameters can be changed in real-time to observe their effect in real-time and also for fine tuning of parameters in real-time. Experimental results in steady-state and transient operation for all the four proposed control schemes are obtained by executing the appropriate MATLAB/SIMULINK files and models. Experimental

results c scheme

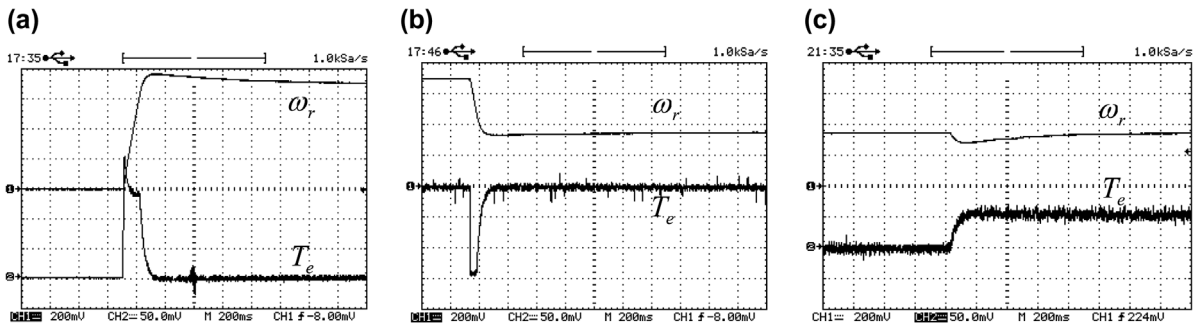

Figure 10. Experimental results of rotor speed ω_r (20 rad/s/div) and torque T_e (4 N m/div) for proposed DTC scheme based on slip angle control transient responce for: (a) during acceleration, (b) deaccelerate to half of the rotor speed and (c) step load torque condition.

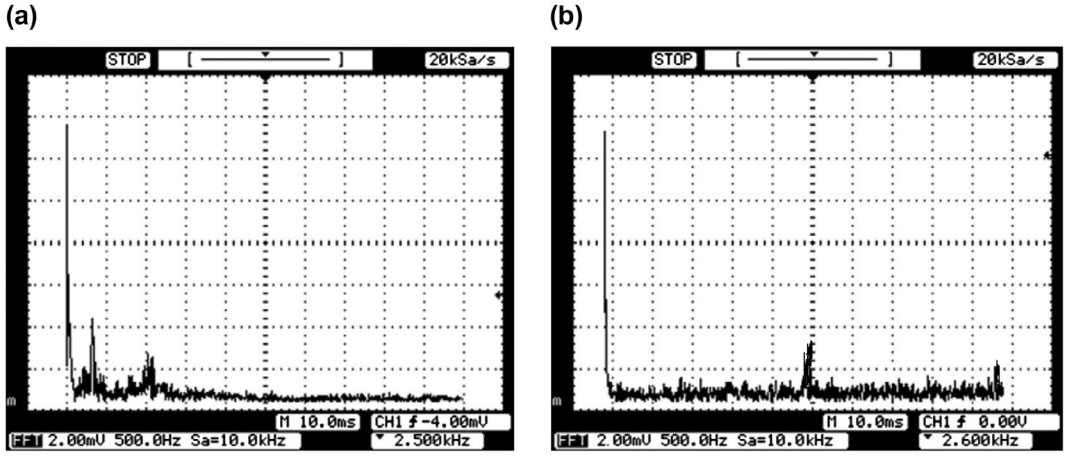

Figure 11. Frequency spectrum of the phase voltage: (a) conventional-DTC and (b) proposed DTC scheme based on slip angle control.

on slip angle control schemes are shown from Figures 6 to 10. The experiments are carried out for various loads but results are shown for 60% of rated load as a sample.

Figure 6 shows the stator phase current for conventional DTC and proposed DTC schemes. Figure 6(a) is simulated phase current in conventional DTC whereas Figure 6(b) shows experimental result. Figure 6(c) gives simulated phase current of proposed DTC whereas Figure 6(d) gives phase current of proposed DTC through experimentation. Figure 7 shows the simulated and experimental results of stator flux locus for conventional DTC and proposed DTC, respectively. The transient response of conventional DTC and proposed DTC scheme based on slip angle control induction motor drive is observed by sudden application of load and results are shown from Figures 8 to 10. The experiments are carried out for various step loads but results are shown for 60% of rated load. Figure 8 shows the speed and torque transient response for conventional DTC and proposed DTC scheme based on slip angle control schemes.

Figure 8(a) and (c) shows simulated response of speed and torque in forward motoring (70 rad/s) for a step change in load torque of conventional and proposed slip angle controlled DTC respectively. Figure 8(b) and (d) demonstrate experimental response of speed and torque in forward motoring (70 rad/s) for a step change in load torque of conventional and proposed slip angle controlled DTC, respectively. Figure 9 shows the stator flux and speed response due to speed reversal based on slip angle control schemes. Figure 10 presents the speed transient for proposed DTC scheme.The experimental results from Figures 6 to 9 show that the torque ripple and flux ripple are less in proposed DTC when compared with conventional DTC. In proposed DTC, the required voltage space vector is calculating to compensate the flux and torque errors exactly by using a predictive technique and then its generation using the SVM at each sample period. Figures 8 and 9 show the transient behavior of drive for step variation of the load torque and speed reversal. Figure 8 shows that there is a sudden reduction in the speed due to sudden increase in load, resulting in reduction in speed. To meet the load torque, the angle between stator flux and rotor flux increases due to selection of accelerating voltage vector which results in increase in motor torque, as a result the motor accelerates till motor torque becomes equal to the load torque and the motor regain its initial reference speed. From Figure 9 it is noticed that the stator flux amplitude of the conventional-DTC and DTC based on slip angle control schemes is unaffected during speed changes. From Figure 10 shows the transient and dynamic response of proposed DTC scheme. In comparison with Figure 11(a) and (b), for the conventional DTC, the SVM-DTC increases the inverter switching frequency. As shown in Figure 11(b), the inverter switching frequency is constant. In Figure 11(b), the phase voltage harmonic spectrum of proposed DTC shows that the harmonics are more at inverter switching frequency (2.5 kHz) and its multiples, whereas in conventional DTC the

phase voltage harmonics are more at lower frequencies. Hence, proposed slip angle controlled DTC gives less harmonics when compared to conventional DTC-SVM. The stator flux ripple and torque ripple obtained with the conventional DTC are higher than those obtained with the DTC based on slip angle control and torque transient response of DTC based on slip angle control is close to conventional DTC. From these results it is observed that the DTC based on slip angle control technique offers the less torque ripple and flux ripple in simulation and experimentation.

6. Conclusion

To reduce the torque and flux ripple of the DTC induction motor drive based on slip angle scheme was proposed. Mathematical models were developed and simulation studies were carried out using MATLAB/SIMULINK for proposed DTC scheme. The conventional DTC and proposed DTC of induction motor drive were simulated. Simulation studies are performed under steady state and transient operation. These studies established not only the feasibility of the proposed schemes and also ability to reduce the torque and flux ripple of induction motor drive when compared with conventional DTC scheme. In order to validate the simulation results, experiments were conducted under steady state and transient operations by using dSPACE 1104 controller. From these results it is observed that the proposed DTC technique offered less torque ripple and flux ripple both in simulations and experimentation and also the switching frequency of the inverter had to be kept constant for improving steady state torque and flux response of induction motor drive by using proposed DTC technique. The proposed DTC preserved conventional DTC transient merits, furthermore produced better quality in steady-state flux and torque response. The torque and stator flux ripple of proposed DTC was significantly reduced.

Disclosure statement

No potential conflict of interest was reported by the authors.

Notes on contributors

K. V. Praveen Kumar received his BTech degree in Electrical and Electronics Engineering from Jawaharlal Nehru Technological University, Kakinada, India, in 2011 and MTech, degree from JNTU, Kakinada, India, in 2014. He is presently doing research in the area of Power Electronics and Drives at National Institute of Technology, Warangal, India.

T. Vinay Kumar received his BTech degree in Electrical and Electronics Engineering from Jawaharlal Nehru Technological University, Hyderabad, India, in 2005 and MTech, degree from JNTU, Hyderabad, India, in 2008. He received his PhD degree from National Institute of Technology, Warangal, India, in 2014. Since 2013, he is working as an assistant professor in National Institute of Technology, Warangal, India. He published many research papers in national and international journals and conferences. His research interests are power electronics and drives, multi level inverters and renewable energy.

S. Srinivasa Rao received his BTech degree in Electrical Engineering from Regional Engineering College, Warangal, India, in 1992 and MTech degree from Regional Engineering College, Calicut, India, in 1994. He obtained his PhD degree from National Institute of Technology, Warangal in 2007. Since 1996, he is working as a faculty member in National Institute of Technology, Warangal, India. He published many research papers in national and international journals and conferences. His research interests include power electronic drives, switch mode power converters, DSP-controlled drives and renewable energy generation. He is a life member in System Society of India, Indian Society of Technical Education, member in Institution of Engineers (India) and life fellow in Society of Power Engineers (India).

References

[1] Blaschke F. The principle of field-orientation as applied to the transvector closed-loop control system for rotating-field machines. Siemens Rev. 1972;34(5):217–220.
[2] Takahashi I, Noguchi T. A new quick-response and high-efficiency control strategy of an induction motor. IEEE Trans Ind Appl. 1986;IA-22(5):820–827.
[3] Casadei D, Profumo F, Tani A, et al. FOC and DTC: two viable schemes for induction motors torque control. IEEE Trans Power Electron. 2002;17(5):779–787.
[4] Huy HL. Comparison of field-oriented control and direct torque control for induction motor drives. In: Proceedings of IEEE Conference on Industry Applications. Vol. 2; Canada; 1999. p. 1245–1252.
[5] Nash JN. Direct torque control, induction motor vector control without an encoder. IEEE Trans Ind Appl. 1997;33(2):333–341.
[6] Kang JK, Ki Sul S. New direct torque control of induction motor for minimum torque ripple and constant switching frequency. IEEE Trans Ind Applicat. 1999;35(5):1076–1082.
[7] Habetler TG, Profumo F, Pastorelli M, et al. Direct torque control of induction machines using space vector modulation. IEEE Trans Ind Applicat. 1992;28(5):428–436.
[8] Casadei D, Sera G, Tani A. Stator flux vector control for high performance induction motor drives using space vector modulation. In: Proceedings of OPTIM; Brasov (Romania); 1996. p. 1413–1422.
[9] Xue X, Xu X, Habetler TG, et al. A low cost stator flux oriented voltage source variable speed drive. In: Proceedings of IAS. Vol. 1; Seattle, WA; 1990. p. 410–415.
[10] Lee K-B, Song J-H, Choy I, et al. Improvement of low-speed operation performance of DTC for three-level inverter-fed induction motors. IEEE Trans Ind Electron. 2001;48(5):1006–1014.
[11] Noguchi T., Yamamoto M. Enlarging switching frequency in direct torque-controlled inverter by means of dithering. IEEE Trans Ind Appl. 1999;35(6):1358–1366.
[12] Buja GS, Kazmierkowski MP. Direct torque control of PWM inverter-fed AC motors – a survey. IEEE Trans Power Electron. 2004;51(4):744–757.
[13] Abdelli R, Rekioua D, Rekioua T. Performances improvements and torque ripple minimization for VSI fed induction machine with direct control torque. ISA Trans. 2011;50(2):213–219.
[14] Rumzi Nik Idris N, Halim Mohamed Yatim A. Direct torque control of induction machines with constant switching frequency and reduced torque ripple. IEEE Trans Ind Electron. 2004;51(4):758–767.
[15] Mukherjee S., Poddar G. Direct torque control of squirrel cage induction motor for optimum current ripple using three-level inverter. IET Power Electron. 2010;3(6):904–914.
[16] Patil UV, Suryawansh HM, Renge MM. Torque ripple minimization in direct torque control induction motor drive using space vector controlled diode clamped multi-level inverter. T& F Electric Power Comp Sys. 2012;40(7):792–806.
[17] Vinay Kumar T, Srinivasa Rao S. Modeling and simulation of direct torque controlled induction motor drive using slip speed control. Int J Model Simul. 2013;33(2):109–116.
[18] Vinay Kumar T, Srinivasa Rao S. Direct torque controlled induction motor drive based on cascaded three two-level inverters. Int J Model Simul. 2014;34(2):70–82.
[19] Beerten J, Verveckken J, Driesen J. Predictive direct torque control for flux and torque ripple reduction. IEEE Trans Ind Electron. 2010;57(1):404–412.

[20] Kuo-Kai S, Juu-Kuh L, Van-Truong P, et al. Evolution of local to global minimum torque ripples of direct torque control for induction motor drives. T& F J Chinese Inst Eng. 2012;36(5):608–615.
[21] Korlinchaka C, Comanescu M. Robust sensorless sliding mode flux observer with speed estimate for induction motor drives. T & F J Electric Power Comp Sys. 2012;40(9):1030–1049.
[22] Chatterjeea D. A magnetization curve based stator resistance and fuzzy rotor resistance adaptation technique suitable for speed sensorless field-oriented control of induction machine. T & F J Electric Power Comp Sys. 2012;40(16):1789–1807.
[23] Kashif SAR, Saqib MA. A neuro fuzzy application: soft starting of induction motors with reduced energy losses. T & F J Electric Power Comp Sys. 2012;40(12):1339–1350.
[24] Hajian M., Soltani J., Markadeh GRA. Non-linear direct torque control of sensorless induction motor drives with parameter identification and capable for very low speeds. Electric Power Comp Sys. 2012;40(15):1656–1675.
[25] Kim JS., Sul SK. A novel voltage modulation technique of the space vector PWM. IEE Trans Japan. 1996;116-D(8):820–825.
[26] Zhang J, Rahman MF. Analysis and design of a novel direct flux control scheme for induction machine. In: Proceedings of ICEMD; San Antonio; 2005. p. 426–430.
[27] Vinay Kumar T., Srinivasa Rao S. Hardware implementation of direct load angle controlled induction motor drive. Electric Power Comp Sys. 2014;42(14):1505–1516.

Appendix 1

Specifications of induction machine used for simulation and experimentation:

Table A1. Parameters of Induction machine.

Name	Symbol	Quantity
Stator resistance	R_s	2.23 Ω
Rotor resistance	R_r	1.15 Ω
Stator inductance	L_s	0.21 H
Rotor inductance	L_r	0.21 H
Mutual inductance	L_m	0.1988 H
Poles	P	4
Inertia	J	0.051 kg/m^2
Power	P	2.2 kW
Torque	T	12 N m
Nominal speed	N_r	1440 RPM